

Check for updates

Achieving Uniform Ti/P Co-Modifications for Optimized Li⁺ **Transport Kinetics of LiCoO**₂

Changfa Sun, Hengyu Ren, Xiaohu Wang, Haocheng Ji, Haocong Yi, Wenguang Zhao, Lin Zhou, Qinghe Zhao,* and Feng Pan*

Recently, the deteriorated Li⁺ transport kinetics of LiCoO₂ (LCO) due to the presence of uneven surface coatings and dopants has long puzzled researchers. Herein, by using the hydrolysis of tetrabutyl titanate (C₁₆H₃₆O₄Ti), the interaction between LCO and LiH₂PO₄ is effectively regulated, constructing uniform Li₃PO₄ deposit and Ti-enriched rocksalt (RS) phase on the surface of TP-LCO. The ultrathin Ti-enriched RS phase can effectively stablize the surface lattice oxygen and enhance Li+ transport kinetics, suppressing the Co/O loss and structural collapse. Simultaneously, the uniformly distributed Li₃PO₄ deposits serve as a substrate that facilitates the formation of the reinforced and P-enriched cathode-electrolyte interphase (CEI), ensuring the long-term cycling structural stability. Benefiting from the synergistic effect of uniform bilayer structure, TP-LCO presents a high capacity of 181.7 mA h g^{-1} at the current of 8 C in the TP-LCO/Li cell, and a high capacity retention of 90.9% after 600 cycles at the current of 1 C in the TP-LCO/graphite cell.

1. Introduction

Over the past few decades, lithium-ion batteries, as high-energydensity energy storage devices, have been widely utilized in portable electronic products and electric vehicles, becoming an indispensable part of daily life.[1-4] Among the reported cathode materials, LiCoO2 (LCO) dominates the 3C electronics market due to its high volumetric energy density and excellent conductivity.^[5] However, with the development of science and

C. Sun, H. Ren, X. Wang, H. Yi, W. Zhao, L. Zhou, F. Pan School of Advanced Materials

Peking University Shenzhen Graduate School

Shenzhen518055, China E-mail: panfeng@pkusz.edu.cn

Tsinghua-Berkeley Shenzhen Institute & Tsinghua Shenzhen International Graduate School

Tsinghua University Shenzhen518055, China

College of Physics and Energy Fujian Normal University Fuzhou350117, China

E-mail: katong880109@163.com

The ORCID identification number(s) for the author(s) of this article can be found under https://doi.org/10.1002/adfm.202506727

DOI: 10.1002/adfm.202506727

technology, there is a growing demand for higher energy-density batteries.[6-8] Expanding the voltage window of LCO is the most direct and effective method to achieve higher energy density. For instance, when the cut-off charge voltage increases to 4.6 V (vs Li/Li+), the discharge capacity of LCO can reach 220 mA h g⁻¹, which is a significant improvement compared to the currently used 4.45 V LCO (<190 mA h g⁻¹), demonstrating a rational approach to achieving high-energy-density LCO cathodes.

However, upon high cut-off voltage operation, detrimental structural degradation and rapid capacity fading occur on the LCO. In a deeply delithiated state, intense hybridization between Co 3d and O 2p orbitals takes place, causing electron extraction from O2-, and triggering an oxygen redox reaction from O^{2-} to O^{n-} (0 < n < 2),

leading to oxygen loss and side reactions with the electrolyte. [9-12] Furthermore, the heterogeneous Li⁺ (de)intercalation processes exacerbate an irreversible phase transition (i.e., $CoO_2 \rightarrow Co_3O_4$), resulting in increased impedance and capacity decay.[13] Additionally, when the voltage exceeds 4.55 V, the irreversible phase transition from O3 to H1-3 results in the contraction and sliding of the O-Co-O layer along the c-axis, which leads to steplike degradation (SSD) and crack formation.[14,15] Consequently, the structure decay issues of LCO originate from the surface and further aggravate the bulk phase degradation, so the structural design of the LCO surface is considered an effective strategy to simultaneously achieve high capacity and excellent cycling performances.[16]

Surface coating strategies based on different types of elements have been widely reported. Through these strategies, atomicscale modifications were achieved, leading to the optimization of the material's fundamental physicochemical properties. Elements such as Ti, Mg, Al, F, and P have been demonstrated to be effective in improving the material properties.^[15,17–20] Among these, Ti and P are included in the range of the most promising modifying elements due to its low cost, abundant availability, and non-toxicity. [21] Currently, the optimized mechanisms reported in the literature regarding Ti can be categorized into the following aspects: First, Ti segregation at grain boundaries and surfaces facilitates uniform strain distribution within particles, thereby preventing crack formation.^[9] Second, Ti is doped in the surface or the bulk phase to form stronger Ti-O bonds, thus stabilizing the

1616203. 2025, 44, Downloaded from https://advanced.onlinelibtrary.viely.com/doi/10.1002/admf202506727 by University Town Of Shenzhen, Wiley Online Library on [1711/1025]. See the Terms and Conditions (https://onlinelibrary.wiley.com/terms-and-conditions) on Wiley Online Library or rules of use; OA articles are governed by the applicable Creative Commons License

www.afm-journal.de

lattice oxygen. [22] Third, the formation of solid electrolytes such as $\text{LiTi}_2(\text{PO}_4)_3$, $\text{Li}_{1.5}\text{Al}_{0.5}\text{Ti}_{1.5}(\text{PO}_4)_3$ has demonstrated excellent performance when coated on cathode materials. [23–25] Additionally, P is frequently reported to form the protective Li_3PO_4 surface coating, effectively mitigating interfacial side reactions. [26] Despite the above-mentioned progress, the interaction between the modified elements and LCO during the synthesis process, particularly the mutual effects of multi-element modification, remains unclear. Thus, clarifying the synergistic effects of multiple modified elements during synthesis is of great significance for guiding the development of LCO cathode materials.

Herein, we successfully achieve the construction of a uniform, highly Li⁺- conductive Ti-enriched RS phase and homogeneous Li₃PO₄ deposits on the surface of TP-LCO, utilizing the synergistic effect of Ti(OH)₄·2H₂O (hydrolysis of tetrabutyl titanate) and LiH₂PO₄ during the solution treatment process to regulate the degree of Li+/H+ exchange, followed by moderate-temperature sintering. The uniformly distributed Ti-enriched RS phase and Li₃PO₄ coating layer enhance the surface Li⁺ transport kinetics, and ensures the homogeneity of Li⁺ (de)intercalation. Moreover, benefiting from the formation of stronger Ti-O bonds, it avoids the degradation issues of Co/O loss and structural collapse. Upon cycles, the uniform Li₃PO₄ substrate facilitates the formation of a robust LiF/Li₃PO₄-containing cathode-electrolyte interphase (CEI) on the TP-LCO. Owing to the comprehensive surface modification, TP-LCO exhibits a high capacity of 181.7 mA h g⁻¹ at an 8 C current rate (in TP-LCO/Li cells, 1 C = 200 mA g^{-1}) and maintains 90.9% capacity retention after 600 cycles at 1C (in TP-LCO/graphite cells).

2. Result and Discussion

2.1. Structure and Morphology

In this work, to well understand the benefit roles of uniform surface modification, we synthesize three kinds of samples, including the pristine LCO (LCO), the Li₃PO₄ modified LCO (P-LCO), and the Ti/P co-modified LCO (TP-LCO), and the synthesis process is clarified in detail in the Experimental Section (Supporting Information). As characterized by X-ray diffraction analysis (XRD) (Figure S1, Supporting Information), both the LCO, P-LCO, and TP-LCO display *R-3m* layered structures without any impurity phases. The Rietveld refinement results (Figure 1a; Figure S2 and Tables S1–S3, Supporting Information) further show that the lattice parameters retain nearly the same, indicating that the surface treatment does not alter the bulk structure of LCO.

Scanning electron microscopy (SEM) reveals that the pristine LCO exhibits a near-spherical morphology with a smooth and clean surface, and with a D_{50} value of $\approx 5 \, \mu m$ (Figure S3, Supporting Information). For P-LCO, when treated with LiH₂PO₄ alone, the SEM results show some corrosion and uneven coating appearing on the surface. (Figure S4, Supporting Information). We consider that the decrease in pH during the LiH₂PO₄ solution treatment can lead to the above surface corrosion. In contrast, the surface of TP-LCO displays a dense and uniform surface coating (Figure S5, Supporting Information). For TP-LCO, the solution containing hydrolysis product of tetrabutyl titanate (i.e., Ti(OH)₄·2H₂O) can be utilized as a pH buffer (Figure S6,

Supporting Information), regulating the solution pH and thereby inducing controlled modifications to the surface structure of TP-LCO (Equation S1, Supporting Information). Furthermore, the X-ray photoelectron spectroscopy (XPS) result (Figure S7, Supporting Information) reveals the Ti existence on the surface of TP-LCO.^[27] Moreover, the XPS etching results (Figure S8, Supporting Information) qualitatively indicate that Ti can partly diffuse into the near-surface Co—O lattice of LCO, while P is mainly distributed on the surface region, and the specific distribution of elements requires more precise characterization of individual LCO particles.

High-resolution transmission electron microscopy (HRTEM) results further elucidate the surface structure of TP-LCO. Differing from the well-defined layered structure of LCO (Figure S9, Supporting Information), the surface of TP-LCO exhibits a multi-phase structure character (Figure 1b). Fast Fourier transform (FFT) analysis is further performed on the selected areas in Figure 1b (I for the outermost layer, II for the surface, and III for the bulk phase). The FFT result from region III exhibits a pure layered structure, while region II exhibits the uniformly distributed RS phase with a thickness of ≈5 nm. Compared to the layered phase, the RS phase exhibits a disordered arrangement of Li and Co on the cation lattice, serving as an O-stabilizing layer.[28] Meanwhile, EDS results indicate a significant Ti enrichment in the surface RS region (Figure \$10, Supporting Information), which is consistent with previous literature, introducing high-valence cations can benefit to form RS phase on the LCO surface. [29-31] In addition, we supplement density functional theory (DFT) calculations to evaluate the stability of lattice oxygen with and without Ti doping, and several configurations have been constructed for the rocksalt phase of LCO with Ti doping, and three oxygen sites that correspond to different local environments have been selected for the evaluation. As shown in Figure S11 (Supporting Information), for all configurations after delithiation, the Ti doping will always lead to higher formation energy for an oxygen vacancy, as compared to the case without Ti doping, which suggests the high thermodynamic stability of the Tidoped rocksalt phase. FFT results from region I (Figure 1b) can be indexed as Li₃PO₄. To further prove this point, the TP-LCO particles are directly dispersed on Cu mesh and then characterized by HRTEM, which further confirms the existence of uniform Li₃PO₄ coating on the surface of TP-LCO (Figure S12, Supporting Information).

In contrast, P-LCO exhibits surface corrosion and inhomogeneous ${\rm Li_3PO_4}$ distribution, leading to structural non-uniformity across the material surface. HRTEM shows that, in some localized regions, the surface of P-LCO displays a thick and uneven RS phase layer, while in other regions, the layered phase still persists beneath the agglomerated ${\rm Li_3PO_4}$ deposits (Figure S13, Supporting Information). In order to further verify the composition of Ti/P surface coating on TP-LCO, a 20% scale-up coating experiment is performed. The characteristic XRD peaks of ${\rm Co_3O_4}$ and ${\rm Li_3PO_4}$ can confirm the excessive Li⁺/H⁺ exchange during LiH₂PO₄/LCO interaction (Figure S14, Supporting Information), $^{[32]}$ resulting in the formation of substantial Li⁺-deficient regions in the surface of TP-LCO, and the conversion of phosphate or hydrogen phosphate group to ${\rm Li_3PO_4}$.

As described above, the schematic diagram of the synthesis process for P-LCO and TP-LCO is illustrated in Figure 1c. Surface

16163028, 2025, 44, Downloaded from https://advanced.onlinelibrary.wiley.com/doi/10.1002/adfm.202506727 by University Town Of Shenzhen, Wiley Online Library on [17/11/2025]. See the Terms

inditions) on Wiley Online Library for rules of use; OA articles are governed by the applicable Creative Commons

www.afm-journal.de

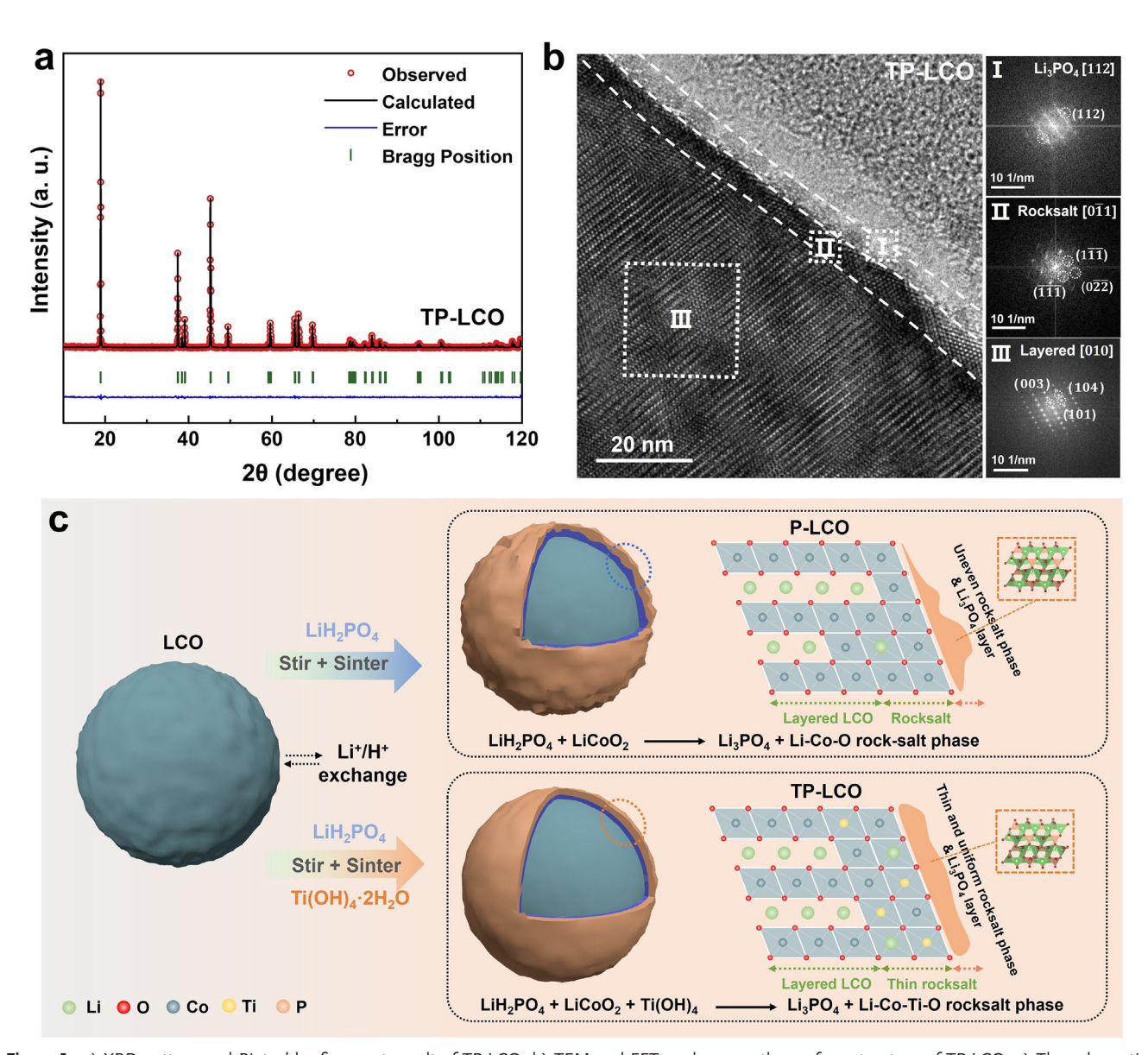


Figure 1. a) XRD pattern and Rietveld refinement result of TP-LCO. b) TEM and FFT analyses on the surface structure of TP-LCO. c) The schematic diagram of the synthesis process for P-LCO and TP-LCO.

treatment of LCO using solely LiH_2PO_4 solution (P-LCO) leads to non-uniform LCO/solution interactions (i.e., Li^+/H^+ exchange), resulting in heterogeneous RS phase and uneven Li_3PO_4 coating layer formation. Upon introducing $Ti(OH)_4 \cdot 2H_2O$ (TP-LCO), the near-neutral solution environment promotes homogeneous LCO/solution interactions, which enables the formation of a uni-

form, thin RS phase structure with evenly distributed Li₃PO₄ coating. Based on the above analyses, the structure features of three kinds of LCO samples are summarized in **Table 1**. For TP-LCO, the surface Li₃PO₄ acts as both a good Li⁺ conductor and the participant for the formation of robust CEI, and the surface Ti-enriched RS acts as the lattice O stabilizer upon high-voltage

 $\textbf{Table 1.} \ \textbf{Illustration of the surface structure features of three samples}.$

Sample	Treatment	Surface structure
LCO	-	Pure layered phase
P-LCO	LiH ₂ PO ₄	Uneven distribution of RS phase and layered phase
TP-LCO	LiH ₂ PO ₄ +Ti(OH) ₄	Uniform and thin (5 nm) Ti-enriched RS layer with $\rm Li_3PO_4$ surface coating

onlinelibrary.wiley.com/doi/10.1002/adfm.202506727 by University Town Of Shenzhen, Wiley Online Library on [17/11/2025]. See the Terms and Conditions (https://originals.com/doi/10.1002/adfm.202506727 by University Town Of Shenzhen, Wiley Online Library on [17/11/2025]. See the Terms and Conditions (https://originals.com/doi/10.1002/adfm.202506727 by University Town Of Shenzhen, Wiley Online Library on [17/11/2025]. See the Terms and Conditions (https://originals.com/doi/10.1002/adfm.202506727 by University Town Of Shenzhen, Wiley Online Library on [17/11/2025]. See the Terms and Conditions (https://originals.com/doi/10.1002/adfm.202506727 by University Town Of Shenzhen, Wiley Online Library on [17/11/2025].

conditions) on Wiley Online Library for rules of use; OA articles are governed by the applicable Creative Commons License

www.afm-journal.de

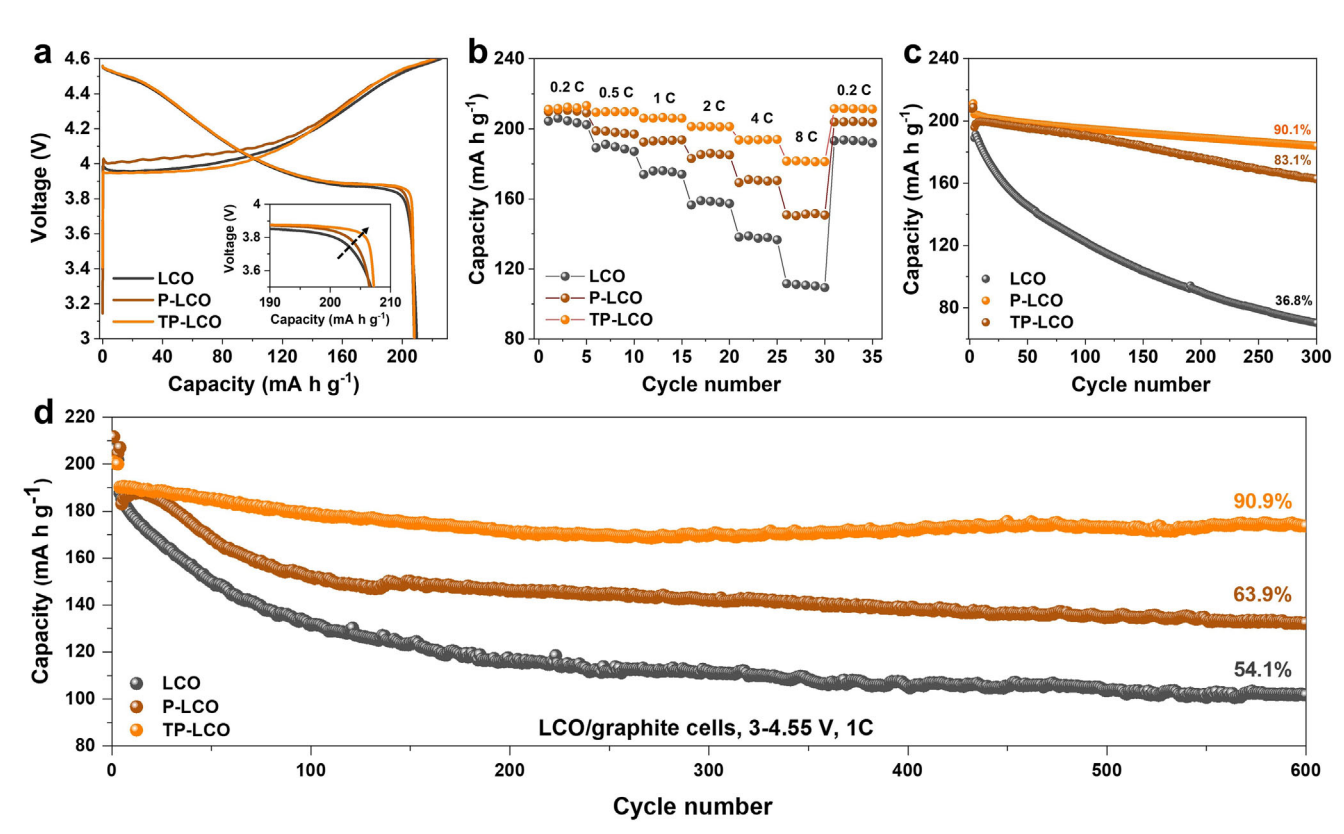


Figure 2. Electrode performances of LCO/Li cells, P-LCO/Li cells, and TP-LCO/Li cells at 25 °C. a) Charge–discharge curves within a voltage range of 3–4.6 V at 0.2 C. b) Comparison of rate performances. c) Comparison of cycle stability in LCO/Li cells in 3–4.6 V, at the current of 1 C. d) Comparison of cycle stability in LCO/graphite cells in 3–4.55 V, at the current of 1 C.

operations. The synergistic effects of multiple factors play a crucial role in stabilizing surface structure and facilitating Li⁺ transport kinetics.

2.2. Electrode Performance

To assess the beneficial role of Ti/P modification, the electrode performances of samples are evaluated in LCO/Li cells and LCO/graphite cells at room temperature (25 °C). The selection of P sources is significant for the surface treatment. At the beginning, two kinds of P sources are selected, including LiH2PO4 and H₃PO₄, and the molar ratio of P/Co is selected as 0.5%. The results reveal that, in LCO/Li cells, the LiH2PO4-LCO exhibits a higher capacity of 200 mA h g^{-1} at 1 C (1 C = 200 mA g^{-1}) with 95.6% capacity retention in 100 cycles, while the H₃PO₄-LCO only shows the lower capacity of 190 mA h g⁻¹ at 1 C with 93.2% capacity retention in 100 cycles (Figure \$15, Supporting Information). As noted, compared with LiH₂PO₄-LCO, H₃PO₄-LCO displays obvious capacity activation in the initial 3 cycles, mainly due to the more extensive Li+/H+ exchange process induced by H₃PO₄, which leads to the more serious surface deterioration of LCO, and results in reduced Li+ transport kinetics of surface structure. Thus, LiH₂PO₄ is selected as the P source for surface modification of LCO. Subsequently, based on the same P contents, the amount of tetrabutyl titanate for the LCO coating process is also investigated, and the results show that, TP- LCO with 0.25% Ti and 0.5% P shows the highest 1 C capacity (203.4 mA h g^{-1}) and highest capacity retention (92.1%) in 200 cycles (Figure S16, Supporting Information).

The charge/discharge curves of LCO/Li cells at the current of 0.2 C are compared in Figure 2a. The results indicate that, as the surface properties vary from LCO to P-LCO and TP-LCO, the discharge curves display progressively increased voltage plateaus, i.e., the reduced polarization, showing the progressively enhanced Li⁺ transport kinetics. Besides, the initial Coulombic efficiency (ICE) values also gradually increase from 92.8% to 93.4% and 94.1%, respectively, indicating the reduced interface side reactions (Figure S17a-c, Supporting Information). Meanwhile, the 1st charge curve of P-LCO shows a higher charging plateau than the following cycles, mainly due to the uneven distribution of Li₃PO₄ and thick RS phase on the surface of P-LCO (Figure \$17b, Supporting Information). For TP-LCO, there exists a good overlap of the charge/discharge curves in initial cycles, indicating enhanced surface structure stability (Figure S17c, Supporting Information).

To reveal the facilitated Li⁺ transport kinetics of TP-LCO, the rate performances are further compared, as shown in Figure 2b. The results indicate that TP-LCO shows the best rate performance, with a high discharge capacity of 181.7 mA h g⁻¹ at 8 C, which is significantly better than that of LCO (109.3 mA h g⁻¹) and P-LCO (150.7 mA h g⁻¹). Additionally, we further carry out Ti-surface-modified LCO (T-LCO) (Figure S18, Supporting Information), and the results show that T-LCO exhibits more

ADVANCED
FUNCTIONAL
MATERIALS

16163028, 2025, 44, Downbaded from https://advanced.onlinelibrary.wiley.com/doi/10.1002/adfm.202506727 by University Town Of Shenzhen, Wiley Online Library on [17/11/2025]. See the Terms and Conditions (https://onlinelibrary.wiley.com/

and-conditions) on Wiley Online Library for rules of use; OA articles are governed by the applicable Creative Commons License

superior rate performance than that of LCO and P-LCO, but is inferior than that of TP-LCO, highlighting the synergistic effect of surface P and Ti on facilitating the Li⁺ transport kinetics.

The cycle stability is further performed to evaluate the effectiveness of the Ti/P-optimized surface structure. Figure 2c compares the cycle performances of LCO, P-LCO, and TP-LCO electrodes at a current of 1 C, tested in LCO/Li cells. The results show that TP-LCO maintains a capacity retention of 90.1% after 300 cycles at 1 C, which is much higher than that of P-LCO (retention of 83.1%), and significantly better than that of the LCO (retention of 54.1%). Moreover, the evolution of both charge/discharge average voltages and the Coulombic efficiency indicate severe interfacial side reactions and structural degradation in LCO during long-term cycling, while TP-LCO maintains excellent structural stability. (Figure \$19, Supporting Information). In addition, TP-LCO also exhibits remarkable electrochemical stability in both high-mass-loading electrodes (Figure S20, Supporting Information) and elevated-temperature cycling at 45 °C (Figure S21, Supporting Information).

To clarify the practical usage of TP-LCO, the cycle of LCO/graphite full cells is further performed within a voltage range of 3–4.55 V (Figure 2d). The results indicate that, in LCO/graphite cells, TP-LCO displays excellent cycle stability, with a capacity retention of 90.9% after 600 cycles at 1C, which is significantly higher than the 63.9% retention of P-LCO, and far superior to the 54.1% retention of LCO. Combining the above results, the electrode performances of TP-LCO are quite competitive among the recently reported high-voltage LCO cathodes (Table S4, Supporting Information). In addition, these results clearly illustrate the synergistic effect of Ti/P modification, which considerably optimizes the surface and interface structure, resulting in stabilized and facilitated Li⁺ transport kinetics for TP-LCO. More discussions will be carried out subsequently to elaborate on the beneficial mechanism of surface Ti/P modification.

2.3. Enhanced Li+ Transport Kinetics

As described above, Ti/P modification benefits a lot on both the stabilized structure and facilitated Li⁺ transport kinetics of TP-LCO. In order to explore the facilitated Li⁺ transport kinetics, electrochemical impedance spectroscopy (EIS) and cyclic voltammetry (CV) are tested, utilizing the LCO/Li cells, which can sensitively characterize the interface reactions of LCO.[33,34] The EIS of LCO/Li cells consistently exhibit three characteristic features, i.e., two semicircles and one slope tail, corresponding to impedance of surface film resistance (R_{st}) , charge transfer resistance (R_{ct}) at the surface, and the Li+ ion diffusion resistance in the structure, respectively.[35] The EIS diagrams can be further analyzed in the form of distribution of relaxation times (DRT) results (Figure S22, Supporting Information), which can further decouple the intertwined electrochemical steps, i.e., R_{CEI} and R_{SEI} . The results show that the change in the value of R_{sf} mainly comes from the evolution of R_{CEI} , demonstrating the critical role of interface and surface structure in both structural stability and Li⁺ transport kinetics of LCO.[36]

As illustrated in Figure 3a-c, the in situ EIS measurements in the 2nd cycle are conducted, and the fitting results (Figure S23,

Supporting Information) display much lower $R_{\rm sf}$ values for TP-LCO compared to that of LCO and P-LCO, indicating a more conductive and superior CEI for the interface Li⁺ transport. Besides, we also observe that the R_{cl} value of TP-LCO is also much smaller than that of LCO. We consider that the constructed double-layer surface of TP-LCO can effectively prevent the rapid degeneration in the near-surface, thus enabling a stabilized and facilitated surface and interface Li⁺ transport kinetics. Even after long-term cycles, this stabilized and facilitated Li⁺ transport kinetics of TP-LCO can still be well retained (Figure S24, Supporting Information).

Figure 3d–f display the CV curves in the initial 5 cycles within the voltage range of 3–4.6 V, and with a scan rate of 0.2 mV s⁻¹. As the cycle proceeds, the redox peak spacing ($\triangle V$) values for LCO, P-LCO, and TP-LCO are 0.228, 0.186, and 0.168 V, respectively. The results indicate a gradually decreased tendency of $\triangle V$ values, reflecting the gradually decreased surface polarization. Besides, the CV measurements at various scan rates (from 0.4 to 1.4 mV s⁻¹) between 3 and 4.6 V are used to further evaluate the Li⁺ diffusion kinetics, as shown in Figure S25 (Supporting Information). The kinetics behavior can be fitted by the formula of i = av^b , in which i represents the peak current of the anode/cathode peaks (mA g^{-1}), ν represents the scanning rates (mV s^{-1}), and the closer the *b* value is to 1, the better the Li⁺ ions diffusion kinetics of cathodes.[31] The fitting results (Figure 3g-i) show that the b values of the anodic and cathodic plots for TP-LCO are 0.78 and 0.87, respectively, which are significantly higher than that of LCO (0.48 and 0.57) and P-LCO (0.61 and 0.66), indicating that TP-LCO has the best Li+ transport kinetics. The enhanced Li+ transport kinetics can be further characterized by the galvanostatic intermittent titration technique (GITT).^[37] In initial cycles, TP-LCO demonstrates a slightly higher Li⁺ diffusion coefficient (D_{Li+}) than that of LCO (Figure S26, Supporting Information). After 100 cycles, the D_{Ii+} of LCO decreases significantly, indicating the severely surface deterioration upon cycles, while the $D_{i,\perp}$ of TP-LCO increases obviously, indicating the formation of reinforced CEI upon cycle, which can be confirmed by the increased R_{sf} values and nearly unchanged R_{ct} values for TP-LCO in different cycles (Figure S24, Supporting Information). Combining all the EIS, CV, and GITT results, the facilitated Li⁺ transport kinetics of TP-LCO is confirmed. More characterizations of CEI and near-surface structure will be carried out in the following sections, aiming to reveal the interfacial evolution of TP-LCO during cycling.

2.4. Regulated CEI Formation

The formation of robust CEI plays an important role in enhancing the performance of LCO. [38,39] Therefore, we further analyze the CEI layers of LCO and TP-LCO after 100 cycles at the current of 1 C, and the morphology and composition of the CEI are characterized using HRTEM, as shown in **Figure 4a**–d. As observed, the CEI on the LCO surface exhibits a thin and uneven character, with numerous defects and irregular protrusions, due to the excessive side reactions between LCO and electrolyte (Figure 4a). Besides, in some regions, the thickness of CEI is less than 5 nm, and it displays an almost amorphous state (Figure 4b), which greatly deteriorates the Li⁺ conductivity of CEI. In contrast, the

nelibrary.wiley.com/doi/10.1002/adfm.202506727 by University Town Of Shenzhen, Wiley Online Library on [17/11/2025]. See the Terms

nditions) on Wiley Online Library for rules of use; OA articles are governed by the applicable Creative Commons

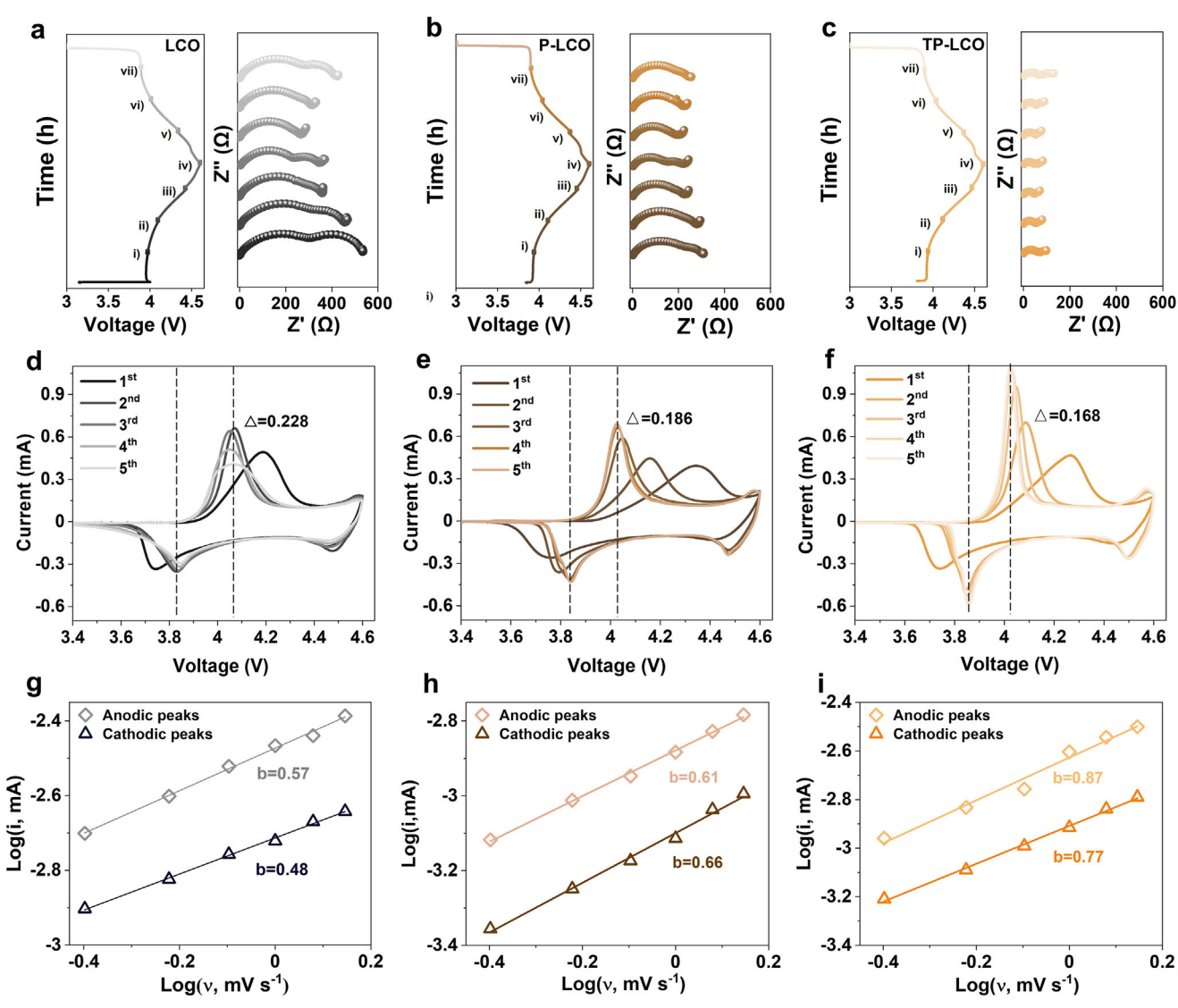


Figure 3. Comparison of the Li⁺ transport kinetics of LCO, P-LCO, and TP-LCO. a–c) Comparison of in situ EIS curves in the 2nd cycles in LCO/Li cells under 25 °C. d–f) CV tests within a voltage range of 3–4.6 V at a constant voltage scanning of 0.2 mV s⁻¹. g–i) The b value is calculated by the CV curve of LCO/Li cell at 25 °C from 0.4 to 1.4 mV s⁻¹.

CEI of TP-LCO displays a remarkably uniform and dense character (Figure 4c), with a thickness of ≈ 20 nm, covering homogeneously on the surface (Figure 4d). In addition, the diffraction spots representing the LiF (400) plane and Li₃PO₄ (002) plane are observed in the CEI of TP-LCO, and the corresponding EDS mapping results clearly indicate the formation of a uniform P-enriched CEI on the surface of TP-LCO after 100 cycles (Figure 4e).

XPS is further employed to investigate the detailed composition of CEI on surfaces of both LCO and TP-LCO. In Figure S27 (Supporting Information), the O 1s, F 1s, and P 2p spectra for CEI of LCO and TP-LCO are analyzed, respectively. Plenty of organic species exist in CEI of LCO, due to the solvents' oxidation by the highly oxidative $\text{Co}^{4+}/\text{O}^{\text{n-}}$ (0<n<2). The solvents' decomposition can also aggravate the hydrolysis of LiPF $_6$ salt, leading to the formation of some inorganic species (such as $\text{Li}_x\text{PF}_v\text{O}_z$, etc.), and

causing more Co dissolution from LCO, as shown in the coupled plasma-optical emission spectroscopy (ICP-OES) results on the Li anode side (Figure S28, Supporting Information). [40] For TP-LCO, more inorganic species (Li₃PO₄ and LiF) exist in CEI, and nearly no Co signal exists on the Li anode side, indicating that the Ti/P modification can effectively reduce the decomposition of solvents and Co dissolution. Thus, LiPF₆ decomposes exclusively to LiF components at the interface of TP-LCO and avoids the hydrolysis process, which further reinforces the durability of CEI.

The critical role of Ti/P modification in CEI regulation is clearly demonstrated (Figure 4f). For TP-LCO, the Ti/P modification can significantly reduce the interface side reactions, and the uniform Li₃PO₄ substrate facilitates the formation of a uniform and dense LiF/Li₃PO₄-containing CEI on the surface of TP-LCO, which is electrochemically stable and highly conductive, thus

16163028, 2025, 44, Downloaded from https://advanced.onlinelibrary.wiley.com/doi/10.1002/adfm.202506727 by University Town Of Shenzhen, Wiley Online Library on [17/11/2025]. See the Terms and Conditions (https://advanced.onlinelibrary.wiley.com/doi/10.1002/adfm.202506727 by University Town Of Shenzhen, Wiley Online Library on [17/11/2025]. See the Terms and Conditions (https://advanced.onlinelibrary.wiley.com/doi/10.1002/adfm.202506727 by University Town Of Shenzhen, Wiley Online Library on [17/11/2025]. See the Terms and Conditions (https://advanced.onlinelibrary.wiley.com/doi/10.1002/adfm.202506727 by University Town Of Shenzhen, Wiley Online Library on [17/11/2025]. See the Terms and Conditions (https://advanced.onlinelibrary.wiley.com/doi/10.1002/adfm.202506727 by University Town Of Shenzhen, Wiley Online Library on [17/11/2025]. See the Terms and Conditions (https://advanced.onlinelibrary.wiley.com/doi/10.1002/adfm.202506727 by University Town Of Shenzhen, Wiley Online Library.wiley.com/doi/10.1002/adfm.202506727 by University Town Of Shenzhen, Wiley Online Library.wiley.com/doi/10.1002/adfm.20250672 by University Town Of Shenzhen

onditions) on Wiley Online Library for rules of use; OA articles are governed by the applicable Creative Commons License

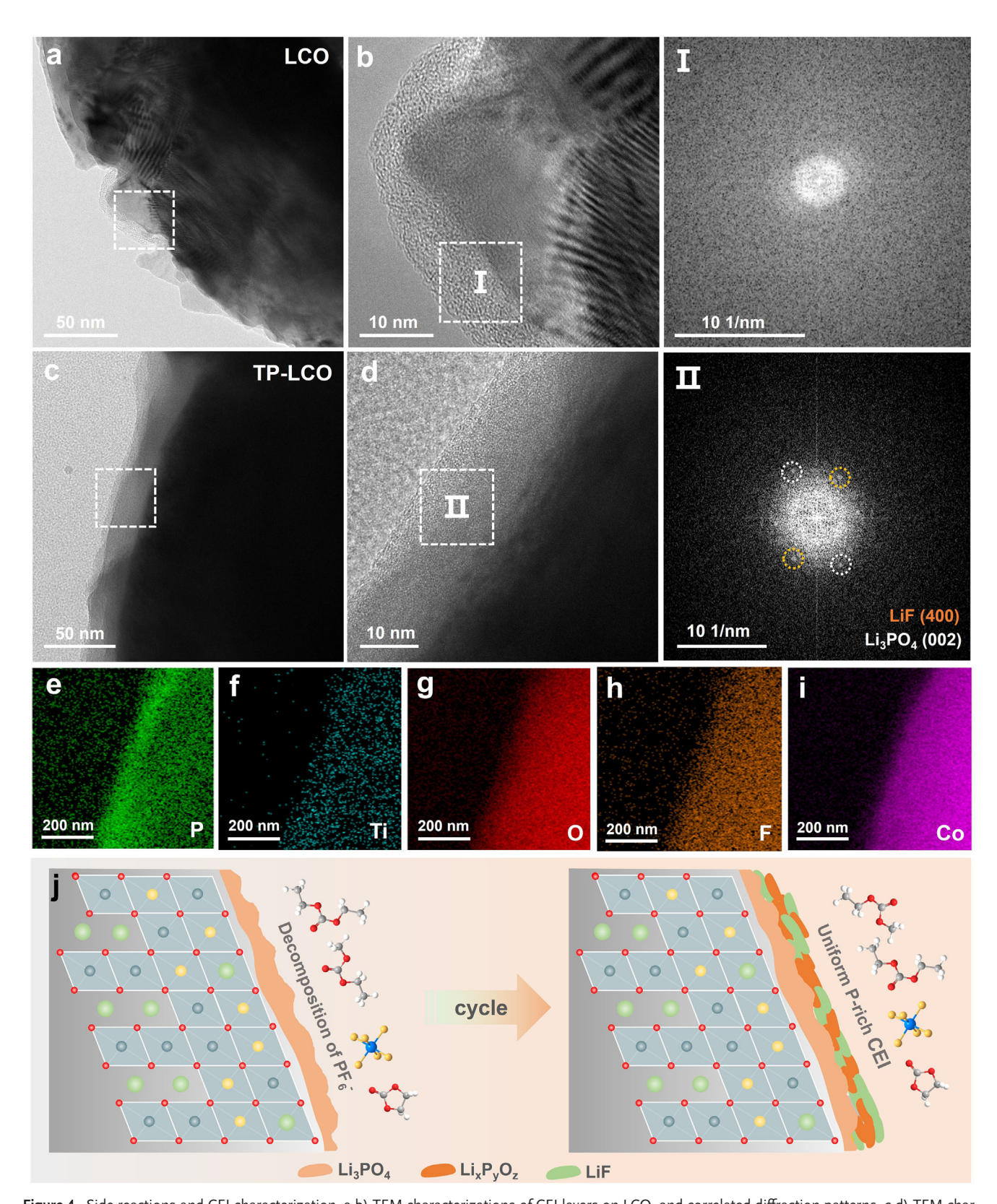


Figure 4. Side reactions and CEI characterization. a,b) TEM characterizations of CEI layers on LCO, and correlated diffraction patterns. c,d) TEM characterizations of CEI layers on TP-LCO, and correlated diffraction patterns. e) EDS mapping of P, Ti, O, F, and Co in the near-surface of TP-LCO. j) The Schematic diagram of CEI evolution on the surface of TP-LCO.

nelibrary.wiley.com/doi/10.1002/adfm.202506727 by University Town Of Shenzhen, Wiley Online Library on [17/11/2025]. See the Terms

nditions) on Wiley Online Library for rules of use; OA articles are governed by the applicable Creative Commons

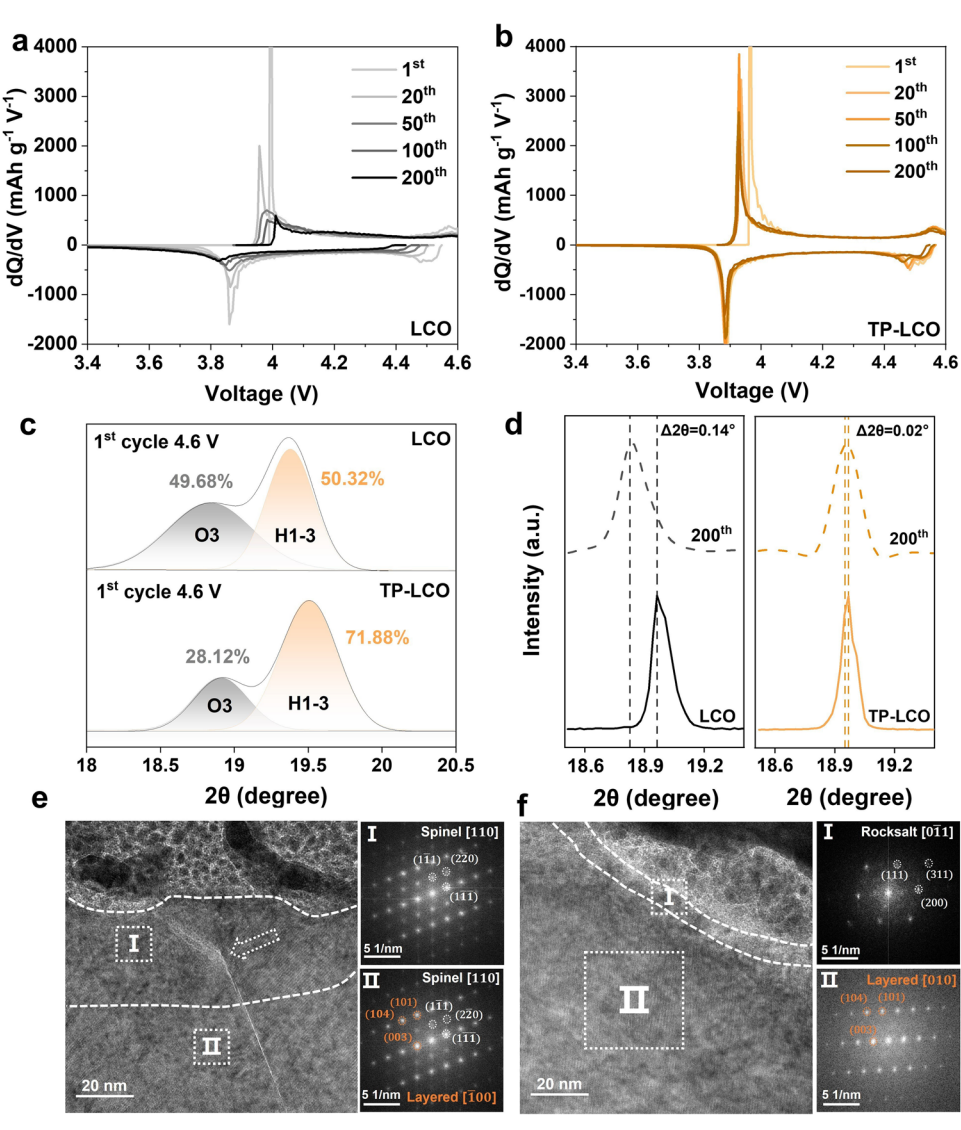


Figure 5. a,b) The dQ/dV curves of LCO and TP-LCO in 200 cycles. c) Comparison of O3/H1-3 transitions of the charged LCO and TP-LCO (at 4.6 V) at 25 °C. d) Variations of (003) peaks of two samples between the pristine and after 200 cycles. e,f) The HRTEM of LCO and TP-LCO and corresponding FFT results after 100 cycles within a voltage range of 3–4.6 V at 1 C.

enhancing the surface stability and interface Li⁺ transport kinetics of TP-LCO.

2.5. Achieving Long-Term Structure Stability

As reported previously, the unprotected LCO surface usually suffers from severe side reactions and structure degradation when operated at high voltage. The structure decay includes the Co/O loss, curvature of Co-O slabs, and inhomogeneous Li⁺ extraction, etc., which finally leads to the irreversible O3/H1-3 phase transitions, and deteriorates the overall stability of LCO particles.^[41–43] The reversibility of O3/H1-3 phase transitions can be reflected by the redox peaks in dQ/dV curves within the voltage range of 4.5–4.6 V (Figure 5a,b).^[13,44] It is evident that the O3/H1-3 phase transition in TP-LCO is more reversible than that in LCO, indicating enhanced phase reversibility due to the Ti/P modification. More-

over, through comparative analysis of the *ex-situ* XRD patterns at the fully charged state (to 4.6 V) in the 1st cycle (Figure 5c), the proportion of H1-3 phase peaks of TP-LCO is calculated as \approx 71.8%, which is higher than that of LCO (\approx 50.32%), indicating that TP-LCO exhibits higher state of charge (SOC) at 4.6 V.

We further characterize the XRD patterns of the cycled LCO and TP-LCO. As shown in Figure 5d, in 200 cycles, the variation of (003) peak for TP-LCO is only 0.017°, which is significantly lower than that of LCO (0.136°), showing more reversible phase transitions and more stable bulk structure of TP-LCO upon long-term cycles. In addition, the difference between XRD patterns of the cycled P-LCO and LCO is nearly invisible, indicating that only applying P modification can hardly enhance the phase durability (Figure \$29, Supporting Information). Thus, as described, an enhanced and more reversible phase transitions can be achieved only upon the synergistic effect of Ti/P modifications.

.com/doi/10.1002/adfm.202506727 by University Town Of Shenzhen, Wiley Online Library on [17/11/2025]. See the Terms and Conditions

onditions) on Wiley Online Library for rules of use; OA articles are governed by the applicable Creative Common

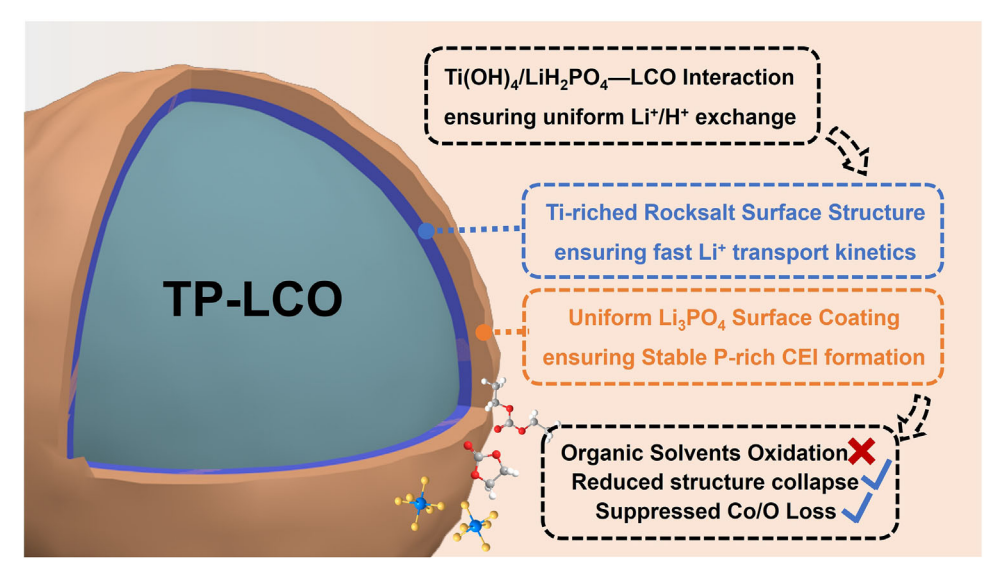


Figure 6. The schematic diagram of the Ti/P modification mechanism.

Figure S30 (Supporting Information) presents the SEM morphology for LCO and TP-LCO electrodes after 100 cycles. It is evident that numerous cracks exist in LCO, while TP-LCO maintains its original characteristics without any crack's generation. HRTEM is further employed to reveal the evolution of surface structures of the cycled LCO and TP-LCO. Figure S31 (Supporting Information) shows the surface structures of LCO and TP-LCO after the 1st cycle. In Figure S31 (Supporting Information), the outermost surface structure of LCO has transformed into a spinel phase, indicating the vulnerable character of the layered phase. In contrast, the surface structure of TP-LCO remains in its pristine state, with a thin Ti-enriched RS phase, which well protects the layered structure in the subsurface.

Figure 5e,f and Figure S32 (Supporting Information) reveal the surface structures of LCO and TP-LCO after 100 cycles. As shown in Figure 5e, a thick spinel phase distributes in the surface (Region I), and an extensive mixed phase of spinel and layered exist in the subsurface (Region II) of LCO. The thickness of this phase transition layer is beyond 50 nm from the surface to the interior of LCO, which seriously blocks the surface Li⁺ transport with large surface impedance (Figure S24, Supporting Information). Besides, due to the uneven delithiation, large cracks are also observed on the surface of LCO after 100 cycles. In contrast, for TP-LCO, the surface structure still remains its pristine state, with the surface Ti-enriched RS phase and the adjacent layered phase distributing in the subsurface and bulk regions (Region II), without detectable cracks' formation (Figure 5f).

Combining the above, the mechanism of uniform Ti/P modification is illustrated in **Figure 6**. To obtain both the stabilized and facilitated Li⁺ transport of LCO, in this work, Ti and P are simultaneously applied to realize the uniform surface Ti-enriched RS phase and surface Li₃PO₄ deposits of TP-LCO. In which, the Ti-enriched RS phase not only acts as an O-stabilizing structure, but also ensures the facilitated surface Li⁺ transport kinetics of TP-LCO, and the Li₃PO₄ deposit enhances the interface Li⁺ transport kinetics and promotes the formation of robust CEI upon cycles. Due to the synthetic effects of Ti/P modification, both the elec-

trolyte decomposition or organic solvent's oxidation, Co/O loss, and structure collapse issues are reduced, thus leading to both superior cycle stability and rate performances.

3. Conclusion

In summary, this study proposes a strategy to optimize both the stability and Li⁺ transport kinetics of LCO. By applying surface optimization, i.e., forming thin Ti-enriched RS phase and uniformly distributed Li₃PO₄ deposits on the surface of TP-LCO, both the cycle stability and rate performances are reinforced. The Ti-enriched RS phase not only acts as an O-stabilizing structure but also ensures the facilitated surface Li⁺ transport kinetics and reduced polarization of TP-LCO. Besides, the surface Li₂PO₄ enhances the interface Li⁺ transport kinetics and promotes the formation of robust P-enriched CEI upon cycles. Benefiting from these surface Ti/P modification, TP-LCO presents a high capacity of 181.7 mA h g⁻¹ at the current of 8 C in TP-LCO/Li cells and shows exceptional stability with 90.9% capacity retention after 600 cycles at 3-4.55 V in TP-LCO/graphite cells. This work provides new insights into the synthesis of advanced LCO cathodes.

Supporting Information

Supporting Information is available from the Wiley Online Library or from the author.

Acknowledgements

C.S. and H.R. contributed equally to this work. This work was financially supported by the International joint Research Center for Electric Vehicle Power Battery and Materials (No. 2015B01015), the Basic and Applied Basic Research Foundation of Guangdong Province (No. 2021B1515130002), the Guangdong Key Laboratory of Design and calculation of New Energy Materials (No. 2017B030301013), and the Shenzhen Key Laboratory of New Energy Resources Genome Preparation and Testing (No. ZDSYS201707281026184).

16163028, 2025, 44, Downloaded from https://advanced.onlinelibrary.wiley.com/doi/10.1002/adfm.202506727 by University Town Of Stenzhen, Wiley Online Library on [17/11/2025]. See the Terms and Conditions (https://doi.org/10.1002/adfm.202506727 by University Town Of Stenzhen, Wiley Online Library on [17/11/2025]. See the Terms and Conditions (https://doi.org/10.1002/adfm.202506727 by University Town Of Stenzhen, Wiley Online Library on [17/11/2025]. See the Terms and Conditions (https://doi.org/10.1002/adfm.202506727 by University Town Of Stenzhen, Wiley Online Library on [17/11/2025]. See the Terms and Conditions (https://doi.org/10.1002/adfm.202506727 by University Town Of Stenzhen, Wiley Online Library on [17/11/2025]. See the Terms and Conditions (https://doi.org/10.1002/adfm.202506727 by University Town Of Stenzhen, Wiley Online Library on [17/11/2025]. See the Terms and Conditions (https://doi.org/10.1002/adfm.202506727 by University Town Of Stenzhen, Wiley Online Library on [17/11/2025]. See the Terms and Conditions (https://doi.org/10.1002/adfm.202506727 by University Town Of Stenzhen, Wiley Online Library on [17/11/2025]. See the Terms and Conditions (https://doi.org/10.1002/adfm.202506727 by University Town Of Stenzhen, Wiley Online Library on [17/11/2025]. See the Terms and Conditions (https://doi.org/10.1002/adfm.202506727 by University Town Of Stenzhen, Wiley Online Library on [17/11/2025]. See the Terms and Conditions (https://doi.org/10.1002/adfm.20250672).

and-conditions) on Wiley Online Library for rules of use; OA articles are governed by the applicable Creative Commons

Conflict of Interest

The authors declare no conflict of interest.

Data Availability Statement

The data that support the findings of this study are available from the corresponding author upon reasonable request.

Keywords

cathode-electrolyte interphase, Li⁺ transport kinetics, LiCoO₂, structure stability, uniform modification

> Received: March 15, 2025 Revised: April 27, 2025 Published online: May 19, 2025

- [1] C. Lin, J. Li, Z. W. Yin, W. Huang, Q. Zhao, Q. Weng, Q. Liu, J. Sun, G. Chen, F. Pan, Adv. Mater. 2023, 36, 2307404.
- [2] Y. Huang, Interdiscip. Mater. 2022, 1, 323.
- [3] W. Li, E. M. Erickson, A. Manthiram, Nat. Energy 2020, 5, 26.
- [4] P. C. J. K. Mizushima, P. J. Wiseman, J. B. Goodenough, Solid State Ionics 1980, 15, 783.
- [5] Y. Lyu, X. Wu, K. Wang, Z. Feng, T. Cheng, Y. Liu, M. Wang, R. Chen, L. Xu, J. Zhou, Y. Lu, B. Guo, Adv. Energy Mater. 2020, 11, 2000982.
- [6] L. Wang, B. Chen, J. Ma, G. Cui, L. Chen, Chem. Soc. Rev. 2018, 47,
- [7] Z. Lin, T. Liu, X. Ai, C. Liang, Nat. Commun. 2018, 9, 5262.
- [8] H. Ren, G. Zheng, Y. Li, S. Chen, X. Wang, M. Zhang, W. Zhao, H. Yi, W. Huang, J. Fang, T. Liu, L. Yang, M. Liu, Q. Zhao, F. Pan, Energy Environ. Sci. 2024, 17, 7944.
- [9] J.-N. Zhang, Q. Li, C. Ouyang, X. Yu, M. Ge, X. Huang, E. Hu, C. Ma, S. Li, R. Xiao, W. Yang, Y. Chu, Y. Liu, H. Yu, X.-Q. Yang, X. Huang, L. Chen, H. Li, Nat. Energy 2019, 4, 594.
- [10] Y. Zhang, Y. Katayama, R. Tatara, L. Giordano, Y. Yu, D. Fraggedakis, J. G. Sun, F. Maglia, R. Jung, M. Z. Bazant, Y. Shao-Horn, Energy Environ. Sci. 2020, 13, 183.
- [11] Y. Chu, Y. Mu, L. Zou, Y. Hu, J. Cheng, B. Wu, M. Han, S. Xi, Q. Zhang, L. Zeng, Adv. Mater. 2023, 35, 2212308.
- [12] X. Wang, H. Ren, Y. Du, Z. Li, W. Zhao, H. Ji, H. Yi, Q. Pan, J. Liu, Z. Lou, L. Zhou, F. Pan, Q. Zhao, Nano Energy 2024, 125, 109537.
- [13] Z. Wu, G. Zeng, J. Yin, C.-L. Chiang, Q. Zhang, B. Zhang, J. Chen, Y. Yan, Y. Tang, H. Zhang, S. Zhou, Q. Wang, X. Kuai, Y.-G. Lin, L. Gu, Y. Qiao, S.-G. Sun, ACS Energy Lett. 2023, 8, 4806.
- [14] A. Fu, Z. Zhang, J. Lin, Y. Zou, C. Qin, C. Xu, P. Yan, K. Zhou, J. Hao, X. Yang, Y. Cheng, D.-Y. Wu, Y. Yang, M.-S. Wang, J. Zheng, Energy Storage Mater. 2022, 46, 406.
- [15] J. Qian, L. Liu, J. Yang, S. Li, X. Wang, H. L. Zhuang, Y. Lu, Nat. Commun. 2018, 9, 4918.
- [16] J. Li, C. Lin, M. Weng, Y. Qiu, P. Chen, K. Yang, W. Huang, Y. Hong, J. Li, M. Zhang, C. Dong, W. Zhao, Z. Xu, X. Wang, K. Xu, J. Sun, F. Pan, Nat. Nanotechnol. 2021, 16, 599.
- [17] Z. Bi, A. Zhang, G. Wang, C. Dong, P. Das, X. Shi, Z.-S. Wu, Sci. Bull. **2024**, *69*, 2071.

- [18] X. Wu, S. Xia, Y. Huang, X. Hu, B. Yuan, S. Chen, Y. Yu, W. Liu, Adv. Funct. Mater. 2019, 29, 1903961.
- [19] C. Liang, F. Kong, R. C. Longo, C. Zhang, Y. Nie, Y. Zheng, K. Cho, J. Mater. Chem. A 2017, 5, 25303.
- [20] H. Ren, W. Zhao, H. Yi, Z. Chen, H. Ji, Q. Jun, W. Ding, Z. Li, M. Shang, J. Fang, K. Li, M. Zhang, S. Li, Q. Zhao, F. Pan, Adv. Funct. Mater. 2023, 33, 2302622.
- [21] Y. Yao, Z. Xue, C. Li, J. Li, J. He, X. Zhang, Y. Xiang, Energy Storage Mater. 2024, 71, 103666.
- [22] L. Wang, J. Ma, C. Wang, X. Yu, R. Liu, F. Jiang, X. Sun, A. Du, X. Zhou, G. Cui, Adv. Sci. 2019, 6, 1900355.
- [23] W. Dong, B. Ye, M. Cai, Y. Bai, M. Xie, X. Sun, Z. Lv, F. Huang, ACS Energy Lett. 2023, 8, 881.
- [24] C. Sun, B. Zhao, R.-d. Cui, J. Mao, K.-H. Dai, H.-Z. Chen, X.-h. Zhang, J.-c. Zheng, ACS Appl. Mater. Interfaces 2023, 15, 21982.
- [25] Y. Wang, Q. Zhang, Z. C. Xue, L. Yang, J. Wang, F. Meng, Q. Li, H. Pan, J. N. Zhang, Z. Jiang, W. Yang, X. Yu, L. Gu, H. Li, Adv. Energy Mater. 2020, 10, 2001413.
- [26] N. Qin, Q. Gan, Z. Zhuang, Y. Wang, Y. Li, Z. Li, I. Hussain, C. Zeng, G. Liu, Y. Bai, K. Zhang, Z. Lu, Adv. Energy Mater. 2022, 12, 202201549.
- [27] J. Li, Z. Zhang, C. Qin, Y. Jiang, X. Han, Y. Xia, M. Sui, P. Yan, Small 2023, 19, 2303474.
- [28] W. Ding, H. Ren, Z. Li, M. Shang, Y. Song, W. Zhao, L. Chang, T. Pang, S. Xu, H. Yi, L. Zhou, H. Lin, Q. Zhao, F. Pan, Adv. Energy Mater. 2024, 14, 2303926.
- [29] X. Tan, Y. Zhang, S. Xu, P. Yang, T. Liu, D. Mao, J. Qiu, Z. Chen, Z. Lu, F. Pan, W. Chu, Adv. Energy Mater. 2023, 13, 2300147.
- [30] X. Cheng, X. Liu, L. Zhao, D. Zhang, J. Biao, Z. Chen, Y. Yuan, M. Liu, Y. B. He, F. Kang, Adv. Funct. Mater. 2022, 33, 202211171.
- [31] Z. Li, W. Zhao, H. Ren, H. Yi, Y. Du, H. Yu, J. Fang, Y. Song, H. Chen, L. Zhou, S. Li, Q. Zhao, F. Pan, Adv. Energy Mater. 2024, 14, 2402223.
- [32] L. Feng, Z. Chen, M. Zhang, S. Zhang, J. Zheng, D. Xiao, C. Liu, Z. Lin, Adv. Funct. Mater. 2024, 34, 202316543.
- [33] J. Zheng, J. Lu, K. Amine, F. Pan, Nano Energy 2017, 33, 497.
- [34] A. Yano, M. Shikano, A. Ueda, H. Sakaebe, Z. Ogumi, J. Electrochem. Soc. 2016, 164, A6116.
- [35] H. Ren, J. Hu, H. Ji, Y. Huang, W. Zhao, W. Huang, X. Wang, H. Yi, Y. Song, J. Liu, T. Liu, M. Liu, Q. Zhao, F. Pan, Adv. Mater. 2024, 36, 202408875.
- [36] Y. Lu, C.-Z. Zhao, J.-Q. Huang, Q. Zhang, Joule 2022, 6, 1172.
- [37] Z. Zhuang, J. Wang, K. Jia, G. Ji, J. Ma, Z. Han, Z. Piao, R. Gao, H. Ji, X. Zhong, G. Zhou, H. M. Cheng, Adv. Mater. 2023, 35, 2212059.
- [38] Z. Zhu, H. Wang, Y. Li, R. Gao, X. Xiao, Q. Yu, C. Wang, I. Waluyo, J. Ding, A. Hunt, J. Li, Adv. Mater. 2020, 32, 2005182.
- [39] H. Ren, X. Wang, W. Ding, C. Xu, W. Zhao, H. Ji, H. Yi, Z. Zhan, Y. Song, L. Zhou, Q. Zhao, F. Pan, Adv. Funct. Mater. 2025, 2504165.
- [40] R. Sim, L. Su, A. Dolocan, A. Manthiram, Adv. Mater. 2023, 36, 2311573.
- [41] J. Xia, N. Zhang, Y. Yang, X. Chen, X. Wang, F. Pan, J. Yao, Adv. Funct. Mater. 2022, 33, 2212869.
- [42] W. Zhang, F. Cheng, M. Chang, Y. Xu, Y. Li, S. Sun, L. Wang, L. Xu, Q. Li, C. Fang, M. Wang, Y. Lu, J. Han, Y. Huang, Nano Energy 2024, 119, 109031.
- [43] J. Chen, H. Chen, S. Zhang, A. Dai, T. Li, Y. Mei, L. Ni, X. Gao, W. Deng, L. Yu, G. Zou, H. Hou, M. Dahbi, W. Xu, J. Wen, J. Alami, T. Liu, K. Amine, X. Ji, Adv. Mater. 2022, 34, 2204845.
- [44] M. Hirooka, T. Sekiya, Y. Omomo, M. Yamada, H. Katayama, T. Okumura, Y. Yamada, K. Ariyoshi, J. Power Sources 2020, 463, 228127.